Four-body resonances of ^{7}B using the complex scaling method

Takayuki Myo,[1,2,*] Yuma Kikuchi,[2,†] and Kiyoshi Katō[3,‡]

[1]*General Education, Faculty of Engineering, Osaka Institute of Technology, Osaka 535-8585, Japan*

[2]*Research Center for Nuclear Physics (RCNP), Osaka University, Ibaraki 567-0047, Japan*

[3]*Division of Physics, Graduate School of Science, Hokkaido University, Sapporo 060-0810, Japan*

(Received 4 November 2011; published 6 December 2011)

We study the resonance spectroscopy of the proton-rich nucleus ^{7}B in the $^4\mathrm{He} + p + p + p$ cluster model. Many-body resonances are treated under the correct boundary condition as Gamow states using the complex scaling method. We predict five resonances of ^{7}B and evaluate the spectroscopic factors of the ^{6}Be-p components. The importance of the $^6\mathrm{Be}(2^+)$-p component is shown in several states of ^{7}B; this is a common feature of ^{7}He, a mirror nucleus of ^{7}B. For only the ground state of ^{7}B, the mixing of the $^6\mathrm{Be}(2^+)$ state is larger than that of $^6\mathrm{He}(2^+)$ in ^{7}He, which indicates a breaking of mirror symmetry. This is caused by the small energy difference between ^{7}B and the excited $^6\mathrm{Be}(2^+)$ state, the origin of which is Coulomb repulsion.

DOI: 10.1103/PhysRevC.84.064306 PACS number(s): 21.60.Gx, 21.10.Dr, 21.10.Pc, 27.20.+n

I. INTRODUCTION

Radioactive beam experiments have provided us with much information on unstable nuclei far from stability. In particular, light nuclei near the drip line exhibit new phenomena of nuclear structures, such as the neutron halo structure found in ^{6}He, ^{11}Li, and ^{11}Be [1]. Unstable nuclei can often be in unbound states beyond particle thresholds due to their weak binding nature. Resonance spectroscopy of unbound states beyond the drip line has also been developed experimentally. In addition to energies and decay widths, configuration properties are important for understanding the structures of the resonances. Spectroscopic factors (S factors) give useful information regarding the configurations of extra nucleons in resonances as well as in weakly bound states. It is also interesting to compare the structures of resonances and weakly bound states between proton-rich and neutron-rich cases. This comparison is related to mirror symmetry in unstable nuclei.

Recently, an experiment on ^{7}B was reported [2], adding to prior observations [3]. The ^{7}B nucleus is known as an unbound system beyond the proton drip line, and its ground state is naively considered to be the $3/2^-$ resonance. The ground state of ^{7}B is observed at 2 MeV above the $^6\mathrm{Be} + p$ threshold energy, and excited states have not yet been observed. ^{7}B states can decay not only to two-body $^6\mathrm{Be} + p$ channels, but also to many-body channels of $^5\mathrm{Li} + 2p$ and $^4\mathrm{He} + 3p$. This multiparticle decay condition makes it difficult to identify the states of ^{7}B experimentally. The mirror nucleus of ^{7}B is ^{7}He, which is also an unbound system with respect to one-neutron emission. Recent experiments on ^{7}He [4–11] confirm that its ground state shows a $3/2^-$ resonance. The S factor of the ^{6}He-n component was reported for the ground state of ^{7}He [10]. The excited states of ^{7}He can decay into the $^4\mathrm{He} + 3n$ channel, which is also difficult to observe experimentally. There still remain contradictions in the observed energy levels of ^{7}He.

From the viewpoint of the "^{4}He plus three protons and/or neutrons" system, information on ^{7}B and ^{7}He is important to understand structures outside the drip lines as four-body pictures. It is also interesting to examine the effect of Coulomb interaction and mirror symmetry in the resonances of two nuclei. Structures of resonances generally depend on the existence of open channels as the thresholds of particle emissions. In this sense, the mirror symmetry of resonances can be related to the behavior of coupling to open channels. It is interesting to compare the effects of couplings to open channels for the resonances of ^{7}B and ^{7}He.

On the theoretical side, to treat unbound states explicitly several methods have been developed, such as the microscopic cluster model [12,13], the continuum shell model [14] and the Gamow shell model [15,16]. It is, however, difficult to satisfy multiparticle decay conditions correctly for all open channels. For ^{7}B, it is necessary to describe $^4\mathrm{He} + 3p$ four-body resonances in theory. So far, no theory describes the ^{7}B nucleus as four-body resonances. It is also important to reproduce the threshold energies of subsystems for particle decays; specifically, the positions of open channels. Emphasizing these theoretical conditions, in this study we employ the cluster orbital shell model (COSM) [17–20] of the $^4\mathrm{He} + 3p$ four-body system. In COSM, the effects of all open channels are taken into account explicitly [19] so that we can treat the many-body decay phenomena. In our previous work on neutron-rich systems [19–21], we successfully described He isotopes with the $^4\mathrm{He} + 4n$ model up to the five-body resonances of ^{8}He, including full couplings with ^{5,6,7}He. We described many-body resonances using the complex scaling method (CSM) [22–24] under correct boundary conditions for all decay channels. In CSM, the resonant wave functions are directly obtained by diagonalization of the complex-scaled Hamiltonian using L^2 basis functions. Results for light nuclei using CSM have been obtained successfully for energies, decay widths, and spectroscopic factors, and also for breakup strengths induced by Coulomb excitations [25,26], monopole transition [21] and one-neutron removal [20]. Recently, CSM has been developed to include nuclear reaction methods such as scattering amplitude calculation [27], the Lippmann-Schwinger equation

*myo@ge.oit.ac.jp
†yuma@rcnp.osaka-u.ac.jp
‡kato@nucl.sci.hokudai.ac.jp

[28], and the continuum-discretized coupled-channel (CDCC) method [29].

In this study, we proceed with our study of resonance spectroscopy of the proton-rich nucleus ^{7}B. We examine how our model describes ^{7}B as four-body resonances. We predict the resonances of ^{7}B and investigate their configuration properties. We extract the S factors of the ^{6}Be-p components for every ^{7}B resonance. The S factors are useful for understanding the coupling behavior between ^{6}Be and the last proton. For the mirror nucleus ^{7}He we have performed the same analysis of the S factors of the ^{6}He-n components [20], in which a large mixing of the ^{6}He(2^+) state is confirmed. From the viewpoint of mirror symmetry, we compare the structures of ^{7}B with those of ^{7}He and discuss the effect of the Coulomb interaction on mirror symmetry. Since the two nuclei are both unbound, the coupling effect of the open channels is discussed.

In Sec. II, we explain the complex-scaled COSM wave function and the method of obtaining the S factors using CSM. In Sec. III, we discuss the ^{7}B structures and the S factors of the ^{6}Be-p components. A summary is given in Sec. IV.

II. COMPLEX-SCALED COSM

A. COSM for ^{4}He + $N_v p$ systems

We use COSM for $^4\mathrm{He} + N_v p$ systems, where N_v is the valence proton number around ^{4}He, namely $N_v = 3$ for ^{7}B. The Hamiltonian form is the same as that used in Refs. [19,20]:

$$H = \sum_{i=1}^{N_v+1} t_i - T_G + \sum_{i=1}^{N_v} V_i^{\alpha p} + \sum_{i<j}^{N_v} V_{ij}^{pp} \tag{1}$$

$$= \sum_{i=1}^{N_v} \left(\frac{\vec{p}_i^{\,2}}{2\mu} + V_i^{\alpha p} \right) + \sum_{i<j}^{N_v} \left(\frac{\vec{p}_i \cdot \vec{p}_j}{4m} + V_{ij}^{pp} \right), \tag{2}$$

where t_i and T_G are the kinetic energies of each particle (p and ^{4}He) and of the center of mass of the total system, respectively. The vector $\vec{p}_i$ is the relative momentum between p and ^{4}He. The reduced mass μ is $4m/5$ using a nucleon mass m. The ^{4}He-p interaction $V^{\alpha p}$ is given by the microscopic KKNN potential [24,30] for the nuclear part, in which the tensor correlation of ^{4}He is renormalized on the basis of the resonating group method in $^4\mathrm{He} + N$ scattering. For the Coulomb part, we use the folded Coulomb potential using the density of ^{4}He with a $(0s)^4$ configuration. We use the Minnesota potential [31] as

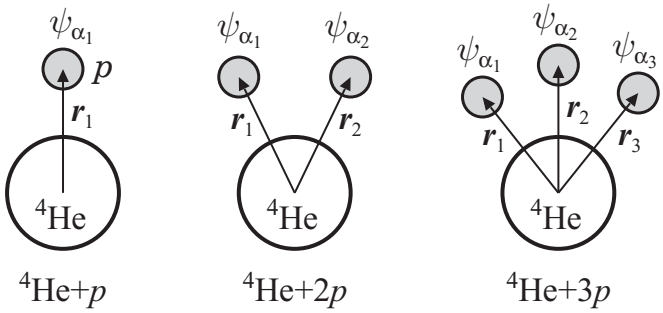

FIG. 1. Sets of the spatial coordinates in COSM for the $^4\mathrm{He} + N_v p$ system.

the nuclear part of V^{pp} in addition to the Coulomb interaction. These interactions reproduce the low-energy scattering of the ^{4}He-N and N-N systems, respectively.

For the wave function, ^{4}He is treated as a $(0s)^4$ configuration of a harmonic-oscillator wave function, whose length parameter is 1.4 fm to fit the charge radius of ^{4}He of 1.68 fm. The motion of valence protons around ^{4}He is solved variationally using the few-body technique. We expand the relative wave functions of the $^4\mathrm{He} + N_v p$ system using the COSM basis states [17–20]. In COSM, the total wave function Ψ^J with spin J is represented by the superposition of the configuration Ψ_c^J as

$$\Psi^J = \sum_c C_c^J \Psi_c^J, \tag{3}$$

$$\Psi_c^J = \prod_{i=1}^{N_v} a_{\alpha_i}^\dagger |0\rangle, \tag{4}$$

where the vacuum $|0\rangle$ is given by the ^{4}He ground state. The creation operator $a_\alpha^\dagger$ is for the single-particle state of a valence proton above ^{4}He with quantum number $\alpha = \{n, \ell, j\}$ in a jj coupling scheme. Here, the index n represents the different radial components. The coefficient C_c^J represents the amplitude of the configuration and its index c represents the set of α_i as $c = \{\alpha_1, \ldots, \alpha_{N_v}\}$. We take a summation over the available configurations in Eq. (3), which gives a total spin J.

The coordinate representation of the single-particle state corresponding to $a_\alpha^\dagger$ is given by $\psi_\alpha(\boldsymbol{r})$ as a function of the relative coordinate $\boldsymbol{r}$ between the center of mass of ^{4}He and a valence proton [17], as shown in Fig. 1. Considering the angular momentum coupling, the explicit wave functions of the COSM configuration Ψ_c^J in Eq. (4) are expressed as

$$\Psi_c^J = \mathcal{A}'\left\{\left[\Phi(^4\mathrm{He}), \chi_c^J(N_v p)\right]^J\right\}, \tag{5}$$

$$\chi_c^J(p) = \psi_{\alpha_1}^J, \tag{6}$$

$$\chi_c^J(2p) = \mathcal{A}\left\{\left[\psi_{\alpha_1}, \psi_{\alpha_2}\right]_J\right\}, \tag{7}$$

$$\chi_c^J(3p) = \mathcal{A}\left\{\left[\left[\psi_{\alpha_1}, \psi_{\alpha_2}\right]_{j_{12}}, \psi_{\alpha_3}\right]_J\right\}. \tag{8}$$

Here, $\Phi(^4\mathrm{He})$ is the ^{4}He wave function with spin 0^+. The function $\chi_c^J(N_v p)$ expresses the COSM wave functions for the valence protons. The spin j_{12} is the coupled angular momentum of the first and second valence protons. The antisymmetrizers between valence protons and between a valence proton and nucleons in ^{4}He are expressed as the symbols $\mathcal{A}$ and $\mathcal{A}'$, respectively. The effect of $\mathcal{A}'$ is treated in the orthogonality condition model [20,24], in which ψ_α is imposed to be orthogonal to the $0s$ state occupied by ^{4}He. We employ a sufficient number of radial bases of ψ_α to describe the spatial extension of valence protons in resonances where ψ_α is normalized. In this model, the radial part of ψ_α is expanded with Gaussian basis functions for each orbit as

$$\psi_\alpha = \sum_{k=1}^{N_{\ell j}} d_\alpha^k \, \phi_{\ell j}^k(\boldsymbol{r}, b_{\ell j}^k), \tag{9}$$

$$\phi_{\ell j}^k(\boldsymbol{r}, b_{\ell j}^k) = \mathcal{N} r^\ell e^{-(r/b_{\ell j}^k)^2/2}\left[Y_\ell(\hat{\boldsymbol{r}}), \chi_{1/2}^\sigma\right]_j. \tag{10}$$

The index k is for the Gaussian basis with length parameter $b^k_{\ell j}$. A normalization factor of the basis and a basis number are given by $\mathcal{N}$ and $N_{\ell j}$, respectively.

In COSM, using Gaussian expansion, the total wave function Ψ^J contains two kinds of expansion coefficients: $\{C^J_c\}$ in Eq. (3) for configuration and $\{d^k_\alpha\}$ in Eq. (9) for each valence proton. We determine them using the following procedure. First, we solve the eigenvalue problem of the norm matrix of the Gaussian basis set in Eq. (10), which is nonorthogonal with dimension $N_{\ell j}$. The coefficients $\{d^k_\alpha\}$ are determined to construct the orthonormalized single-particle basis set $\{\psi_\alpha\}$ having different radial components with number $N_{\ell j}$. Second, Hamiltonian matrix elements are constructed using $\{\psi_\alpha\}$ and are diagonalized to determine $\{C^J_c\}$ from the variational principle. The relation $\sum_c (C^J_c)^2 = 1$ is satisfied due to the normalization of the total wave function. The same method of determining the expansion coefficients using Gaussian bases is used in the tensor-optimized shell model [32].

The numbers of radial bases $N_{\ell j}$ of ψ_α are determined to converge the physical solutions Ψ^J. The length parameters $b^k_{\ell j}$ are chosen in geometric progression [20,24]. We use at most 17 Gaussian basis functions by setting $b^k_{\ell j}$ from 0.2 fm to around 40 fm with the geometric ratio of 1.4 as a typical one. Due to the expansion of the radial wave function using a finite number of basis states, all the energy eigenvalues are discretized for bound, resonant, and continuum states. For reference, in the Gamow shell-model calculation [15,16], the single particle states ψ_α consist of resonant and discretized continuum states obtained with the single-particle potential $V^{\alpha p}$ in Eq. (2).

For ^{7}B, all the channels of $^6\mathrm{Be} + p$, $^5\mathrm{Li} + 2p$, and $^4\mathrm{He} + 3p$ are automatically included in the total COSM wave function Ψ^J. These components are coupled to each other via interactions and antisymmetrization. The couplings depend on the relative distances between ^{4}He and a valence proton and between valence protons. We explain the coupling behavior between ^{4}He and valence protons in COSM. This is related to the boundary condition of the proton emission in ^{7}B, which is important when the resonant and continuum states are treated [19,26,33]. As an example, we consider the coupling between ^{7}B and the $^6\mathrm{Be} + p$ configurations. Asymptotically, when the last proton is located far away from ^{6}Be, namely, $\boldsymbol{r}_3 \to \infty$ as in Fig. 1, any coupling between ^{6}Be and a last proton disappears, and ^{6}Be is described by an isolated eigenstate of the Hamiltonian in Eq. (2) with $N_v = 2$:

$$\Psi^J(^7\mathrm{B}) = \sum_c C^J_c \mathcal{A}'\left\{\left[\Phi(^4\mathrm{He}), \chi^J_c(3p)\right]^J\right\} \tag{11}$$

$$\overrightarrow{\boldsymbol{r}_{3\to\infty}} \left[\Psi^{J'}_\nu(^6\mathrm{Be}), \psi_{\alpha_3}\right]^J, \tag{12}$$

$$\Psi^{J'}_\nu(^6\mathrm{Be}) = \sum_c C^{J'}_{c,\nu} \mathcal{A}'\left\{\left[\Phi(^4\mathrm{He}), \chi^{J'}_{c,\nu}(2p)\right]^{J'}\right\}, \tag{13}$$

where the spins J and J' are for ^{7}B and ^{6}Be, respectively, and the index ν indicates the eigenstate of ^{6}He. The mixing coefficients $\{C^{J'}_{c,\nu}\}$ and the wave function $\chi^{J'}_{c,\nu}(2p)$ in Eq. (13) are those of the ^{6}Be eigenstates. Hence, the wave function $\chi^J_c(3p)$ in Eq. (11) satisfies the following asymptotic form:

$$\sum_c C^J_c \chi^J_c(3p) \overrightarrow{\boldsymbol{r}_{3\to\infty}} \left(\sum_c C^{J'}_{c,\nu} \chi^{J'}_{c,\nu}(2p)\right) \psi_{\alpha_3}. \tag{14}$$

This relation implies that the wave function of the three valence protons of ^{7}B is asymptotically decomposed into ^{6}Be and a last proton. Equations (11)–(14) determine the boundary condition of COSM. In contrast, when a last proton comes close to ^{6}Be, the last proton dynamically couples to the ^{6}Be eigenstates $\Psi^{J'}_\nu$. This coupling depends on the relative distance between ^{6}Be and a last proton, and changes the ^{6}Be configurations from isolated eigenstates of ^{6}Be. In COSM, the structure change of ^{6}Be inside ^{7}B is determined variationally to optimize the ^{7}B eigenstates. The same method is applied to the asymptotic conditions for the $^5\mathrm{Li} + 2p$ and $^4\mathrm{He} + 3p$ configuations. Hence proton emissions can be handled with correct boundary conditions in COSM.

We now explain the parameters of the model space of COSM and the Hamiltonian, which are determined in the previous analyses of He isotopes [19,20]. For single-particle states, we use angular momentum $\ell \leqslant 2$ to keep the accuracy of the converged energy within 0.3 MeV for ^{6}He with the $^4\mathrm{He} + n + n$ model, in comparison with the full-space calculation [24]. In this model, we adjust the two-neutron separation energy of $^6\mathrm{He}(0^+)$ to the experimental result of 0.975 MeV by using the 173.7-MeV value of the repulsive strength from the Minnesota potential instead of the original value of 200 MeV. The adjustment of the NN interaction originates from the pairing correlation between valence protons with higher angular momentum $\ell > 2$ [24]. Hence, the present model reproduces the observed energies of ^{6}He and is applied to the proton-rich nuclei in this analysis.

B. Complex scaling method (CSM)

Here we explain CSM, which describes resonances and nonresonant continuum states [22–24]. Hereafter, we refer to the nonresonant continuum states as simply the continuum states. In CSM, we transform the relative coordinates of the $^4\mathrm{He} + N_v p$ system as $\boldsymbol{r}_i \to \boldsymbol{r}_i e^{i\theta}$ for $i = 1, \ldots, N_v$, where θ is a scaling angle. The Hamiltonian in Eq. (2) is transformed into the complex-scaled Hamiltonian H_θ, and the corresponding complex-scaled Schrödinger equation is given as

$$H_\theta \Psi^J_\theta = E \Psi^J_\theta. \tag{15}$$

The eigenstates Ψ^J_θ are obtained by solving the eigenvalue problem of H_θ in Eq. (15). In CSM, we obtain all the energy eigenvalues E of bound and unbound states on the complex energy plane, governed by the ABC theorem [34]. In this theorem, it is proved that the boundary condition of resonances is transformed to one of damping behavior in the asymptotic region. This condition makes it possible to use the same method to obtain bound states and resonances. For a finite value of θ, every Riemann branch cut starting from the different thresholds is commonly rotated down by 2θ. Hence, continuum states such as the $^6\mathrm{Be} + p$ and $^5\mathrm{Li} + 2p$ channels

in ^{7}B are obtained on the branch cuts rotated by -2θ from the corresponding thresholds [19,20]. In contrast, bound states and resonances are obtainable independent of θ. We can identify resonance poles with complex eigenvalues: $E = E_r - i\Gamma/2$, where E_r and Γ are the resonance energies and the decay widths, respectively. In the wave function, the θ dependence is included in the expansion coefficients in Eqs. (3) and (9) as $\{C_c^J(\theta)\}$ and $\{d_\alpha^k(\theta)\}$, respectively. The value of the angle θ is determined to search for the stationary point of each resonance in the complex energy plane [22–24].

The resonant state generally has a divergent behavior at asymptotic distance, and then its norm is defined by a singular integral using, for example, the convergent-factor method [24,35,36]. In CSM on the other hand, resonances are precisely described as eigenstates expanded in terms of L^2 basis functions. The amplitudes of the resonances are finite and are normalized as $\sum_c (C_c^J(\theta))^2 = 1$. The Hermitian product is not applied due to the bi-orthogonal relation [22,23,37]. The matrix elements of resonances are calculated using the amplitudes obtained in CSM.

In this study, we discretize the continuum states in terms of the basis expansion, as shown in the figures of energy eigenvalue distributions in Refs. [20,24,25]. The reliability of the continuum discretization in CSM has already been shown using continuum level density [38] and phase-shift analysis [27].

C. Spectroscopic factor of ^{7}B

We now explain the S factors of the ^{6}Be-p components for ^{7}B. As was explained in the previous study [20], since the resonant states generally give complex matrix elements, the S factors of resonant states are not necessarily positive definite. The S factors are defined by the squared matrix elements using the bi-orthogonal property [37] as

$$S^{J,\nu}_{J',\nu'} = \sum_\alpha S^{J,\nu}_{J',\nu',\alpha}\,, \tag{16}$$

$$S^{J,\nu}_{J',\nu',\alpha} = \frac{1}{2J+1}\left\langle \widetilde{\Phi}^{J'}_{\nu'} \middle|\middle| a_\alpha \middle|\middle| \Psi^J_\nu \right\rangle^2, \tag{17}$$

where the annihilation operator a_α is for a single valence proton with state α. The spins J and J' are for ^{7}B and ^{6}Be, respectively. The index ν (ν') indicates the eigenstate of ^{7}B (^{6}Be). The wave function $\Phi^{J'}_{\nu'}$ is for ^{6}Be. In this expression, the values of $S^{J,\nu}_{J',\nu'}$ are allowed to be complex. In general, the imaginary parts of the S factors often become large relative to the real parts for a resonance having a large decay width. Recently, the Gamow shell-model calculation was also used to discuss the S factors of resonances [39].

The sum-rule value of the S factors, which includes resonance contributions of the final states, can now be considered [19]. When we count all the S factors, not only of resonances but also of the continuum states in the final states, the summed value of the S factors is equal to the associated particle number, which is a real value and does not contain any imaginary part, similarly to the transition-strength calculation [25,40]. For the ^{7}B into ^{6}Be-p decomposition, the summed value of the S factors $S^{J,\nu}_{J',\nu'}$ in Eq. (17), taking all the ^{6}Be states, is given as

$$\sum_{J',\nu'} S^{J,\nu}_{J',\nu'} = \sum_{\alpha,m} \left\langle \widetilde{\Psi}^{JM}_\nu \middle| a^\dagger_{\alpha,m} a_{\alpha,m} \middle| \Psi^{JM}_\nu \right\rangle = 3, \tag{18}$$

where we use the completeness relation of ^{6}Be as

$$1 = \sum_{J',M'} \sum_{\nu'} \left| \Phi^{J'M'}_{\nu'} \right\rangle \left\langle \widetilde{\Phi}^{J'M'}_{\nu'} \right|. \tag{19}$$

Here M (M') and m are the z components of the angular momenta of the wave functions of ^{7}B (^{6}Be) and of the creation and annihilation operators of the valence protons, respectively. It is found that the summed value of the S factors for the ^{6}Be states becomes the valence proton number N_v of ^{7}B. This discussion of the S factors is valid when complex scaling is used. It is also shown that th S factors of the resonances are invariant with respect to the scaling angle θ [20,36].

The present S factors can be used to obtain the strength of the proton removal reaction from ^{7}B into ^{6}Be as a function of the energy of ^{6}Be. In this calculation, the S factors not only of the resonances but also of the many-body continuum states for ^{7}B and ^{6}Be are necessary. The complex-scaled Green's function is also used to calculate the strength distribution [20,25,41]. In fact, for the neutron-rich case, we have shown the one-neutron removal strength distributions from ^{7}He into ^{6}He states using CSM [20]. The strength of three-body scattering states of ^{6}He into ^{4}He $+ n + n$ was successfully obtained by

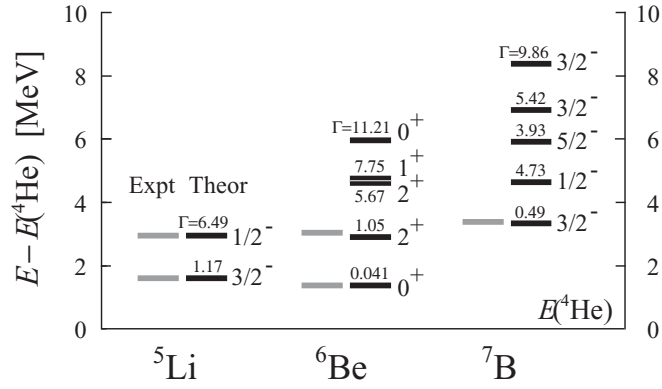

FIG. 2. Energy levels of ^{5}Li, ^{6}Be, and ^{7}B measured from the ^{4}He energy. Units are in MeV. Black and gray lines are theory and experiments, respectively. Small numbers are decay widths.

TABLE I. Energy eigenvalues of the ^{6}Be resonances measured from the ^{4}He $+ p + p$ threshold. The values in parentheses are the experimental ones [42]. Dominant configurations are listed.

	Energy (MeV)	Width (MeV)	Configuration
0^+_1	1.383 (1.370)	0.041(0.092)	$(p_{3/2})^2$
0^+_2	5.95	11.21	$(p_{1/2})^2$
2^+_1	2.90 (3.04)	1.05 (1.16)	$(p_{3/2})^2$
2^+_2	4.63	5.67	$(p_{3/2})(p_{1/2})$
1^+	4.76	7.75	$(p_{3/2})(p_{1/2})$

TABLE II. Components of the ground states of ^{6}Be and ^{6}He.

Configuration	^{6}Be(0_1^+)	^{6}He(0_1^+)
$(p_{3/2})^2$	$0.918 - i0.006$	0.917
$(p_{1/2})^2$	$0.041 + i0.000$	0.043
$(1s_{1/2})^2$	$0.010 + i0.006$	0.009
$(d_{5/2})^2$	$0.024 + i0.000$	0.024
$(d_{3/2})^2$	$0.007 + i0.000$	0.007

using the complex-scaled wave function of ^{6}He. It was shown that the ^{6}He(2^+) resonance generates a sharp peak at around the resonance energy in the distribution.

In the numerical calculation, we express the radial part of the operator a_α in Eq. (17) using a complete set of a valence proton expanded by 40 Gaussian basis functions with a maximum range of 100 fm for each orbit. This treatment is sufficient to converge the S-factor results.

III. RESULTS

A. Energy spectra of ^{5}Li, ^{6}Be, and ^{7}B

We show the systematic behavior of level structures of ^{5}Li, ^{6}Be and ^{7}B in Fig. 2. It is found that the present calculations agree with observed energy levels. We furthermore predict many resonances for ^{6}Be and ^{7}B. We first discuss the structures of ^{6}Be, which are useful for understanding of ^{7}B structures. The ^{6}Be states together with a last proton compose the thresholds of the decay of ^{7}B. It is also interesting to compare ^{6}Be structures with those of ^{6}He, a mirror and a neutron-halo nucleus.

The resonance energies and the decay widths of ^{6}Be are listed in Table I with dominant configurations. The components of each configuration for the ^{6}Be and ^{6}He ground states are listed in Table II, which are the squared values of the amplitudes $\{C_c^J\}$ defined in Eq. (3). We show the summation of the components belonging to the same configurations with different radial components of the valence proton. It is noted that the amplitude of the resonant wave function becomes a complex number and its real part can have a physical meaning when the imaginary part has a relatively small value. It is confirmed that the two ground states show a similar trend of configuration, which is dominated by the p shell. The configurations of the 2_1^+ states of ^{6}Be and ^{6}He are also shown in Table III, where the energy and decay width of ^{6}He(2_1^+) are obtained as $(E_r, \Gamma) = (0.879, 0.132)$ in MeV, measured from the ^{4}He $+ n + n$ threshold. A good correspondence is seen for the two dominant configurations of the 2_1^+ states. These results indicate that mirror symmetry of configurations is well

TABLE III. Dominant components of the 2_1^+ states of ^{6}Be and ^{6}He.

Configuration	^{6}Be(2_1^+)	^{6}He(2_1^+)
$(p_{3/2})^2$	$0.891 + i0.030$	$0.898 + i0.013$
$(p_{3/2})(p_{1/2})$	$0.097 - i0.024$	$0.089 - i0.013$

TABLE IV. Radial properties of the ground states of ^{6}Be and ^{6}He in units of fm, in comparison with the experiments of ^{6}He; labels a–d denote Refs. [43–46], respectively.

	^{6}Be	^{6}He	^{6}He (expt.)
R_m	$2.80 + i0.17$	2.37	2.33(4)[a], 2.30(7)[b], 2.37(5)[c]
R_p	$3.13 + i0.20$	1.82	
R_n	$1.96 + i0.08$	2.60	
$R_{\rm ch}$	$3.25 + i0.21$	2.01	2.068(11)[d]
r_{NN}	$6.06 + i0.35$	4.82	
$r_{\text{c-}2N}$	$3.85 + i0.37$	3.15	
θ_{NN}	75.3	74.6	

kept between ^{6}Be and ^{6}He. Recently, Gamow shell-model calculations were used to discuss p-shell contributions in the $A = 6$ system [39].

The radial properties of ^{6}Be are of interest when discussing the effect of Coulomb repulsion in comparison with ^{6}He, which has a halo structure, although the radius of ^{6}Be can be a complex number because of the resonance. The results of the ^{6}Be ground state are shown in Table IV for matter (R_m), proton (R_p), neutron (R_n), and charge ($R_{\rm ch}$) parts, for the relative distances between valence nucleons (r_{NN}) and between the ^{4}He core and the center of mass of two valence nucleons ($r_{\text{c-}2N}$), and for the opening angle between two nucleons (θ_{NN}) at the center of mass of the ^{4}He core. It is found that the values for ^{6}Be are almost real, so that the real parts can be considered to represent the radius properties of ^{6}Be. The distances between valence protons and between the core and $2p$ in ^{6}Be are wider than those of ^{6}He by 26% and 22%, respectively. This result comes from Coulomb repulsion between the three constituents of ^{4}He $+ p + p$ in ^{6}Be. Coulomb repulsion makes the energy of ^{6}Be shift up to become a resonance in comparison with ^{6}He, and it also increases the relative distances between each constituent from the halo state of ^{6}He.

We now discuss the structures of ^{7}B. The energy eigenvalues are listed in Table V, measured from the ^{4}He $+ 3p$ threshold. We obtained five resonances, which are all located above the ^{6}Be(0_1^+) $+ p$ threshold as shown in Fig. 2, as well as four-body resonances. In Fig. 3 we display the energy eigenvalues of the ^{7}B resonances together with the many-body continuum cuts in the complex energy plane, which is useful for understanding at a glance the positions of poles and the various relative thresholds. The ^{6}Be resonances together with

TABLE V. Energy eigenvalues of the ^{7}B resonances measured from the ^{4}He $+ 3p$ threshold. The values in square brackets are the experimental ones [2]. Dominant configurations are listed.

	Energy (MeV)	Width (MeV)	Configuration
$3/2_1^-$	3.35 [3.38(3)]	0.49[0.80(2)]	$(p_{3/2})^3$
$3/2_2^-$	6.92	5.422	$(p_{3/2})^2(p_{1/2})$
$3/2_3^-$	8.39	9.86	$(p_{3/2})(p_{1/2})^2$
$1/2^-$	5.93	4.73	$(p_{3/2})^2(p_{1/2})$
$5/2^-$	4.63	3.91	$(p_{3/2})^2(p_{1/2})$

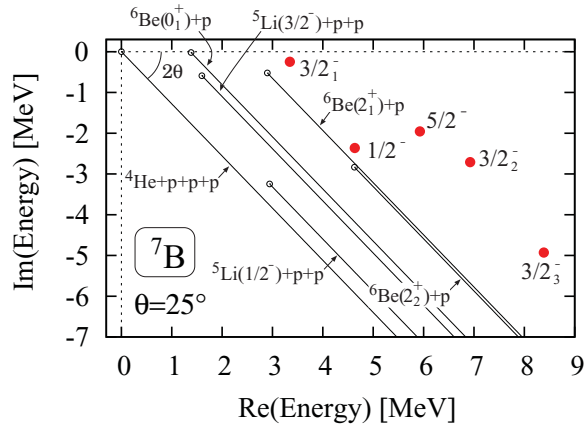

FIG. 3. (Color online) Energy eigenvalue distribution of ^{7}B in the complex energy plane.

a last proton compose the thresholds of ^{7}B, whose positions are located at the starting points of the -2θ-rotated cuts in CSM. The energy of the ^{7}B ground state is obtained as $E_r = 3.35$ MeV, which agrees with the recent experiment result of $E_r = 3.38(3)$ MeV [2]. The decay width is 0.49 MeV, which is good but slightly smaller than the experimental value of 0.80(2) MeV. In the experiment, the decay width was determined from R-matrix theory with the assumption of decay into the ^{6}Be$(0^+_1) + p$ channel. On the other hand, our analysis shows that the ^{6}Be(2^+_1)-p component is important in the ^{7}B ground state, which is found from the S factors of this channel and is suggested from the conventional shell-model calculation [2]. There is no experimental evidence for the excited states of ^{7}B so far, and further experimental data are anticipated.

We now discuss the configuration properties of each resonance of ^{7}B in detail. In Table VI, we list the main configurations with their squared amplitudes $(C^J_c)^2$ from Eq. (3) for each ^{7}B resonance. In general, the squared amplitude of a resonant state can be a complex number, while the total of the squared amplitudes is normalized to unity. The interpretation of the imaginary part in the physical quantity of resonances is still an open problem [36]. In the results for ^{7}B, the amplitudes of the dominant components are almost real values. It is, hence, reasonable to discuss the physical meaning of the dominant components of the resonances in the same way that we discuss the bound state. It is furthermore found that the imaginary parts of the configurations cancel each other for every resonance, and their summations have much smaller imaginary parts. When we consider all the available configurations, the summations conserve unity due to the normalization of the states.

For the $3/2^-$ ground state, the result indicates that the $(p_{3/2})^3$ configuration is dominant with a small mixing of the $p_{1/2}$ component. For the excited $3/2^-_2$ state, one proton occupies the $p_{1/2}$ orbit and the residual two protons in $p_{3/2}$ form a spin of 2^+, which corresponds to the ^{6}Be(2^+_1) configuration as shown in Table III. The ^{6}Be(2^+_1)-p component in the $3/2^-_2$ state of ^{7}B is important from the viewpoint of the S factors. It is also found that two-particle excitation into the $(p_{1/2})^2$ configuration is mixed by about 20%. The $3/2^-_3$ state is dominated by the $(p_{3/2})(p_{1/2})^2$ configuration, in which the $(p_{1/2})^2$ part has the same configuration as ^{6}Be(0^+_2).

The $1/2^-$ state of ^{7}B corresponds to one-particle excitation from the ground state. Its decay width of 4.73 MeV is large, and is comparable to the resonance energy of 5.93 MeV among the five resonances of ^{7}Be. This is confirmed in Fig. 3 by the large ratio of the imaginary part to the real one in the complex energy plane. The large decay width is similar to that of the ^{5}Li$(1/2^-)$ state in the ^{4}He + p system. In comparison with ^{5}Li, whose resonance energy is 2.93 MeV with a decay width of 6.49 MeV, the ^{7}B$(1/2^-)$ state has a smaller decay width. This difference comes from the residual two protons occupying the $p_{3/2}$ orbit in ^{7}B. The attractive contribution between the $p_{1/2}$ proton and other two protons makes the decay width of the $1/2^-$ state smaller. In the $5/2^-$ state, the 2^+ component of $(p_{3/2})^2$ plus $p_{1/2}$ is dominant. This coupling scheme is similar to the $3/2^-_2$ case. In relation to the configuration properties of ^{7}B, it is interesting to examine the ^{6}Be-p components in each ^{7}B state, which is done using S factors.

It is interesting to discuss the mirror symmetry between ^{7}B and ^{7}He consisting of ^{4}He and three valence protons or neutrons. To do this, we show the energy spectra of He isotopes with COSM in Fig. 4, using the Hamiltonian in Eq. (2) without the Coulomb term. The experimental data of ^{7}He$(1/2^-)$ are not fixed [6–11], so we do not include the data in the figure. From Figs. 2 and 4, it is found that the order of energy levels is the same for proton-rich and neutron-rich cases. In the proton-rich case, whole spectra are shifted up, due to Coulomb repulsion, in comparison with those of the neutron-rich case. The displacement energies are about 2.5 MeV for ^{6}Be from ^{6}He and about 4 MeV for ^{7}B from ^{7}He. In Fig. 5, we compare the excitation energy spectra of proton-rich and neutron-rich cases. It is found that good symmetry is confirmed between the corresponding nuclei. The differences of excitation energies for individual levels are less than 1 MeV. The properties of the

TABLE VI. Dominant configurations of three valence protons in ^{7}B resonances with their squared amplitudes $(C^J_c)^2$.

$3/2^-_1$		$3/2^-_2$		$3/2^-_3$	
$(p_{3/2})^3$	$0.923 + i0.002$	$(p_{3/2})^2(p_{1/2})$	$0.795 + i0.032$	$(p_{3/2})(p_{1/2})^2$	$0.770 + i0.053$
$(p_{3/2})(p_{1/2})^2$	$0.020 + i0.004$	$(p_{3/2})(p_{1/2})^2$	$0.195 - i0.035$	$(p_{3/2})^2(p_{1/2})$	$0.182 - i0.050$
$(p_{3/2})^2(p_{1/2})$	$0.021 - i0.007$	$(d_{3/2})^2(p_{3/2})$	$0.006 + i0.001$	$(p_{3/2})^3$	$0.003 - i0.002$
$1/2^-$				$5/2^-$	
$(p_{3/2})^2(p_{1/2})$	$0.969 - i0.000$			$(p_{3/2})^2(p_{1/2})$	$0.957 + i0.006$
$(d_{5/2})^2(p_{1/2})$	$0.018 - i0.002$			$(d_{3/2})(d_{5/2})(p_{3/2})$	$0.015 - i0.003$
$(1s_{1/2})^2(p_{1/2})$	$0.005 + i0.002$			$(d_{3/2})^2(p_{3/2})$	$0.008 - i0.001$

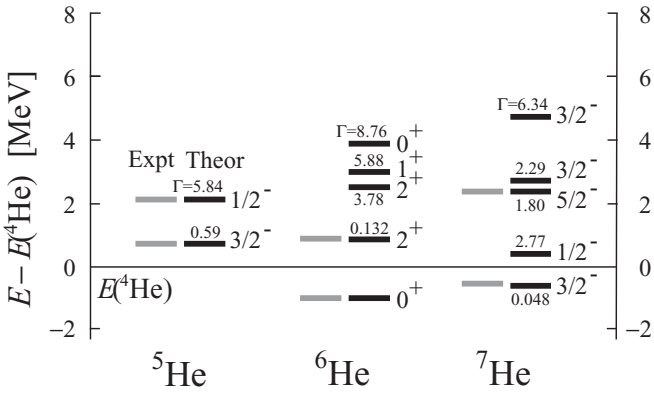

FIG. 4. Energy levels of He isotopes measured from the ^{4}He energy. Units are in MeV. Black and gray lines are theory and experiments, respectively. Small numbers are decay widths.

configurations of ^{7}B and ^{7}He are discussed next in terms of S factors.

B. Spectroscopic factors of ^{7}B

We obtain information on the structures of ^{7}B via S factors. In this study, we extract the S factors of the ^{6}Be-p components in ^{7}B. These quantities is important for examining the coupling behavior between ^{6}Be and a last proton, including the excitations of ^{6}Be. We choose the 0^+_1 and 2^+_1 states of ^{6}Be, which are observed experimentally. In this analysis, both the initial (^{7}B) and final (^{6}Be) states are resonances, so that the S factors become complex numbers. The present S factors correspond to the components of ^{6}Be in the ^{7}B resonances and contain imaginary parts. It is still difficult to derive a definite conclusion regarding the interpretation of the imaginary part in the S factors, as was mentioned in previous studies [20]. Further theoretical and mathematical developments are desired to solve this problem.

In Table VII, we list the results of S factors for ^{7}B. For comparison, the results for ^{7}He are shown in Table VIII. It is found that most of the components show almost real values in ^{7}B and ^{7}He. Hence, a comparison of the real parts of the S factors for ^{7}B and ^{7}He is shown in Figs. 6 and 7.

In Table VII, for the $3/2^-_1$ state, the ^{6}Be(2^+_1)-p component is large: more than four times that of the ^{6}Be(0^+_1)-p component for the real part. This means that the ^{6}Be(2^+_1) state is dominant

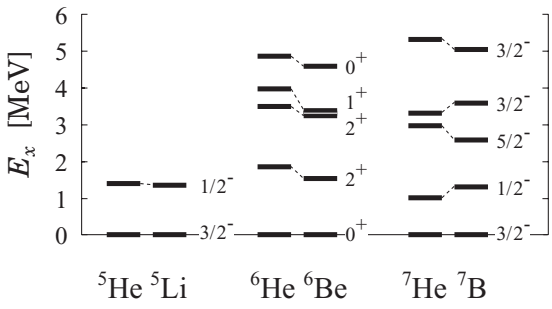

FIG. 5. Excitation energy spectra of mirror nuclei with $A = 5$, 6, and 7 in units of MeV.

TABLE VII. S factors of the ^{6}Be-p components in ^{7}B. Details are described in the text.

	^{6}Be(0^+_1)-p	^{6}Be(2^+_1)-p
$3/2^-_1$	$0.51 + i0.02$	$2.35 - i0.15$
$3/2^-_2$	$0.02 - i0.01$	$0.96 - i0.01$
$3/2^-_3$	$0.00 + i0.01$	$-0.01 - i0.06$
$1/2^-$	$0.93 - i0.02$	$0.10 - i0.01$
$5/2^-$	$0.00 + i0.00$	$1.04 - i0.01$

in this state. A similar trend can be seen in ^{7}He in Table VIII, where the real part of the ^{6}He(0^+_1)-n component agrees with the observation of 0.64(9) [10], as shown in Fig. 6. For the $3/2^-_2$ state, the ^{6}Be(2^+_1)-p component is selectively mixed from the dominant amplitude of $(p_{3/2})^2_{2^+} \otimes (p_{1/2})$. For the $3/2^-_3$ state, the 0^+_1 and 2^+_1 states of ^{6}Be are hardly included because of the $(p_{3/2}) \otimes (p_{1/2})^2$ configuration. Instead of the above two ^{6}Be states—the ^{6}Be(0^+_2) state with $(p_{1/2})^2$ configuration and the ^{6}Be(2^+_2) state with $(p_{3/2})(p_{1/2})$ configuration—one may give large contributions for the $3/2^-_3$ state. For the $1/2^-$ state, the S factor of the ^{6}Be(0^+_1)-$p_{1/2}$ proton is close to unity, with a small imaginary part, and the ^{6}Be(2^+_1)-p component is small. Hence, the ^{6}Be(0^+_1)-p component is dominant in the $1/2^-$ state. The large mixing of the 0^+ state for $A = 6$ nuclei is also confirmed in the ^{7}He$(1/2^-)$ state, as shown in Table VIII. In ^{7}He$(1/2^-)$, we have suggested a weak coupling nature of the $p_{1/2}$ orbital neutron around ^{6}He, which retains a two-neutron halo structure [20]. For the $5/2^-$ state of ^{7}B, the ^{6}Be(2^+_1)-p component is included, similar to $3/2^-_2$ as was explained. These two states have a similar structure of configurations of valence protons. From the S-factor analysis, most of the ^{7}B states are not considered to be purely single-particle states coupled with the ^{6}Be ground state, except for the $1/2^-$ state. The component of ^{6}Be(2^+_1) is important in several states. This conclusion is the same as that for ^{7}He.

We now consider the structure differences between ^{7}B and ^{7}He from the S factors and discuss mirror symmetry. From Fig. 7, a sizable difference between the components including the $A = 6\,(2^+)$ states is seen in the ground states of ^{7}B and ^{7}He. The ^{6}Be(2^+_1)-p component in ^{7}B (obtained as 2.35) is larger than the ^{6}He(2^+_1)-n component in ^{7}He (obtained as 1.60) by 47% for the real part. The other four excited states show similar values between the two nuclei in Figs. 6 and 7. In those excited states, either of the components 0^+ or 2^+ of $A = 6$ nuclei is selectively mixed. These results indicate that the breaking of

TABLE VIII. S factors of the ^{6}He-n components in ^{7}He. Details are described in the text.

	^{6}He(0^+_1)-n	^{6}He(2^+_1)-n
$3/2^-_1$	$0.63 + i0.08$	$1.60 - i0.49$
$3/2^-_2$	$0.00 - i0.01$	$0.97 + i0.01$
$3/2^-_3$	$0.01 + i0.00$	$0.04 - i0.01$
$1/2^-$	$0.95 + i0.03$	$0.07 - i0.02$
$5/2^-$	$0.00 + i0.00$	$1.00 + i0.01$

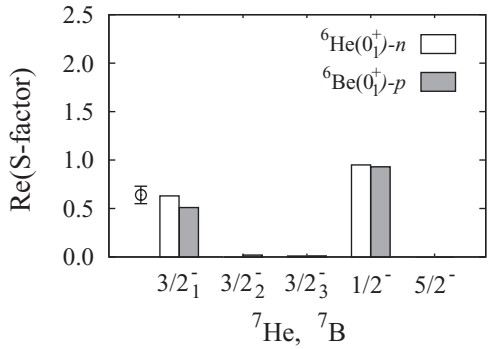

FIG. 6. Real part of the S factors of ^{7}B and ^{7}He, in which the daughter nuclei are the 0^+_1 states. The experimental datum for the ^{7}He($3/2^-$) state [10] is shown by the open circle.

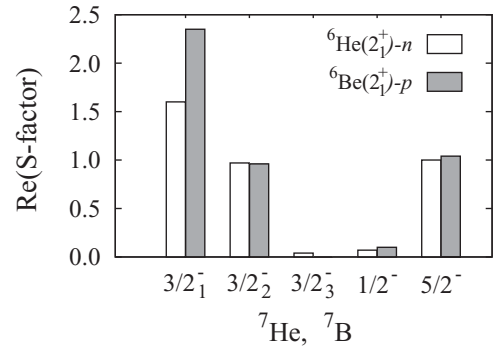

FIG. 7. Real part of the S factors of ^{7}B and ^{7}He, in which the daughter nuclei are the 2^+_1 states.

mirror symmetry occurs only in their ground states. The reason for the difference in the 2^+ coupling is that the ^{7}B ground state is located close to the ^{6}Be(2^+_1) state—within 0.45 MeV for the resonance energy—as shown in Fig. 2 where the decay widths of the two states are rather small in comparison with other resonances. This situation does not occur in ^{7}He, as shown in Fig. 4 where the energy difference between ^{7}He($3/2^-_1$) and ^{6}He(2^+_1) is 1.46 MeV. The small energy difference between ^{7}B and ^{6}Be(2^+_1) enhances the ^{6}Be(2^+_1)-p component in ^{7}B due to the coupling to the open channel of the ^{6}Be(2^+_1) + p threshold. On the other hand, the ^{6}Be(0^+_1)$-p$ component in ^{7}B becomes smaller than that of ^{7}He by 24%, as shown in Fig. 6, because the energy difference between the ground states of ^{7}B and ^{6}Be is 1.97 MeV, larger than 0.40 Mev in the case of ^{7}He. The origin of the difference of the S factors in ^{7}B and ^{7}He is Coulomb repulsion, which acts to shift upward the energies of the ^{7}B states. The well-known effect of the Coulomb interaction to break mirror symmetry is the Thomas-Erhman shift, in which the s-wave dominant states suffer a different effect of Coulomb repulsion from states having mainly other partial waves. On the other hand, the present result found for the ^{7}B ground state is caused by the existence of the several open channels, including the excitations of subsystems, and is different from the Thomas-Erhman shift.

In conclusion, mirror symmetry is broken only in the ground states of ^{7}B and ^{7}He, while the excited states of the two nuclei retain symmetry. This result is associated with the energies of the $A = 6$ subsystem for the open channels of one-nucleon emission. We wish to observe experimentally the 2^+ components of $A = 6$ nuclei in ^{7}B and ^{7}He and examine their mirror symmetry. In the present analysis, the S factors represent the contributions of only the resonances of ^{7}B and ^{6}Be. By considering the additional contributions of the remaining continuum states of the two nuclei, it is possible to obtain the strength functions of one-proton removal from ^{7}B into ^{6}Be and also into ^{4}He + p + p final states, which are observable. It is interesting to obtain these strengths and compare them with the one-neutron removal strength from ^{7}He into ^{6}He [20].

IV. SUMMARY

We have investigated the resonance structures of ^{7}B with the ^{4}He + 3p four-body cluster model. The boundary condition for many-body resonances is accurately treated using the complex scaling method. The decay thresholds concerned with subsystems are described consistently. We have found five resonances of ^{7}B, which are dominantly described by p-shell configurations. The energy and the decay width of the ground state agree with a recent experiment. We also predict four excited resonances of ^{7}B, which we hope to see confirmed experimentally.

We further investigated the spectroscopic factors of the ^{6}Be-p components in ^{7}B to examine the coupling behavior between ^{6}Be and a last proton. It is found that the ^{6}Be(2^+_1) state contributes significantly in the ground state and in several excited states of ^{7}B. In comparison with ^{7}He, the mirror nucleus of ^{7}B, the ^{6}Be(2^+_1)-p component in the ^{7}B ground state is larger than the ^{6}He(2^+_1)-n component in the ^{7}He ground state. This difference comes from the fact that the ^{7}B ground state is close to the ^{6}Be(2^+_1) state in energy, due to Coulomb repulsion. This situation enhances the ^{6}Be(2^+_1)-p component in ^{7}B as channel coupling. The different couplings of $A = 6$ nuclei in ^{7}B and ^{7}He occurred only in their ground states, indicating a breaking of mirror symmetry. We wish to observe the difference of the couplings in ^{7}B and ^{7}He experimentally.

ACKNOWLEDGMENTS

We thank Professor Kiyomi Ikeda for fruitful discussions. This work was supported by a Grant-in-Aid for Young Scientists from the Japan Society for the Promotion of Science (No. 21740194).

[1] I. Tanihata *et al.*, Phys. Rev. Lett. **55** 2676 (1985).
[2] R. J. Charity *et al.*, Phys. Rev. C **84**, 014320 (2011).
[3] L. R. McGrath and J. Cerny, Phys. Rev. Lett. **19**, 1442 (1967).
[4] A. A. Korsheninnikov *et al.*, Phys. Rev. Lett. **82**, 3581 (1999).

[5] H. G. Bohlen, R. Kalpakchieva, A. Blazevic, B. Gebauer, T. N. Massey, W. von Oertzen, and S. Thummerer, Phys. Rev. C **64**, 024312 (2001).
[6] M. Meister *et al.*, Phys. Rev. Lett. **88**, 102501 (2002).
[7] P. Boutachkov *et al.*, Phys. Rev. Lett. **95**, 132502 (2005).
[8] F. Skaza *et al.*, Phys. Rev. C **73**, 044301 (2006).
[9] N. Ryezayeva *et al.*, Phys. Lett. B **639**, 623 (2006).
[10] F. Beck *et al.*, Phys. Lett. B **645**, 128 (2007).
[11] A. H. Wuosmaa *et al.*, Phys. Rev. C **78**, 041302 (2008).
[12] A. Adahchour and P. Descouvemont, Phys. Lett. B **639**, 447 (2006).
[13] K. Arai and S. Aoyama, Phys. Rev. C **80**, 027301 (2009).
[14] A. Volya and V. Zelevinsky, Phys. Rev. Lett. **94**, 052501 (2005).
[15] R. I. Betan, A. T. Kruppa, and T. Vertse, Phys. Rev. C **78**, 044308 (2008).
[16] N. Michel, W. Nazarewicz, and M. Płoszajczak, Phys. Rev. C **75**, 031301 (2007).
[17] Y. Suzuki and K. Ikeda, Phys. Rev. C **38**, 410 (1988).
[18] H. Masui, K. Katō, and K. Ikeda, Phys. Rev. C **73**, 034318 (2006).
[19] T. Myo, K. Katō, and K. Ikeda, Phys. Rev. C **76**, 054309 (2007).
[20] T. Myo, R. Ando, and K. Katō, Phys. Rev. C **80**, 014315 (2009).
[21] T. Myo, R. Ando, and K. Katō, Phys. Lett. B **691**, 150 (2010).
[22] Y. K. Ho, Phys. Rep. **99**, 1 (1983).
[23] N. Moiseyev, Phys. Rep. **302**, 211 (1998).
[24] S. Aoyama, T. Myo, K. Katō, and K. Ikeda, Prog. Theor. Phys. **116**, 1 (2006).
[25] T. Myo, K. Katō, S. Aoyama, and K. Ikeda, Phys. Rev. C **63**, 054313 (2001).
[26] T. Myo, K. Katō, H. Toki, and K. Ikeda, Phys. Rev. C **76**, 024305 (2007).
[27] A. T. Kruppa, R. Suzuki, and K. Katō, Phys. Rev. C **75**, 044602 (2007).
[28] Y. Kikuchi, K. Katō, T. Myo, M. Takashina, and K. Ikeda, Phys. Rev. C **81**, 044308 (2010).
[29] T. Matsumoto, K. Katō, and M. Yahiro, Phys. Rev. C **82**, 051602 (2010).
[30] H. Kanada, T. Kaneko, S. Nagata, and M. Nomoto, Prog. Theor. Phys. **61**, 1327 (1979).
[31] Y. C. Tang, M. LeMere, and D. R. Thompson, Phys. Rep. **47**, 167 (1978).
[32] T. Myo, A. Umeya, H. Toki, and K. Ikeda, Phys. Rev. C **84**, 034315, (2011).
[33] T. Myo, K. Katō, and K. Ikeda, Prog. Theor. Phys. **113**, 763 (2005.
[34] J. Aguilar and J. M. Combes, Commun. Math. Phys. **22**, 269 (1971); E. Balslev and J. M. Combes, *ibid.* **22**, 280 (1971).
[35] W. J. Romo, Nucl. Phys. A **116**, 617 (1968).
[36] M. Homma, T. Myo, and K. Katō, Prog. Theor. Phys. **97**, 561 (1997).
[37] T. Berggren, Nucl. Phys. A **109**, 265 (1968).
[38] R. Suzuki, T. Myo, and K. Katō, Prog. Theor. Phys. **113**, 1273 (2005).
[39] N. Michel, W. Nazarewicz, and M. Płoszajczak, Phys. Rev. C **82**, 044315 (2010).
[40] T. Myo, S. Aoyama, K. Katō, and K. Ikeda, Phys. Lett. B **576**, 281 (2003).
[41] T. Myo, A. Ohnishi, and K. Katō, Prog. Theor. Phys. **99**, 801 (1998).
[42] F. Ajzenberg-selove, Nucl. Phys. A **506**, 1 (1989).
[43] I. Tanihata *et al.*, Phys. Lett. B **289**, 261 (1992).
[44] G. D. Alkhazov *et al.*, Phys. Rev. Lett. **78**, 2313 (1997).
[45] O. A. Kiselev *et al.*, Eur. Phys. J. A **25**, 215 (2005).
[46] P. Mueller *et al.*, Phys. Rev. Lett. **99**, 252501 (2007).